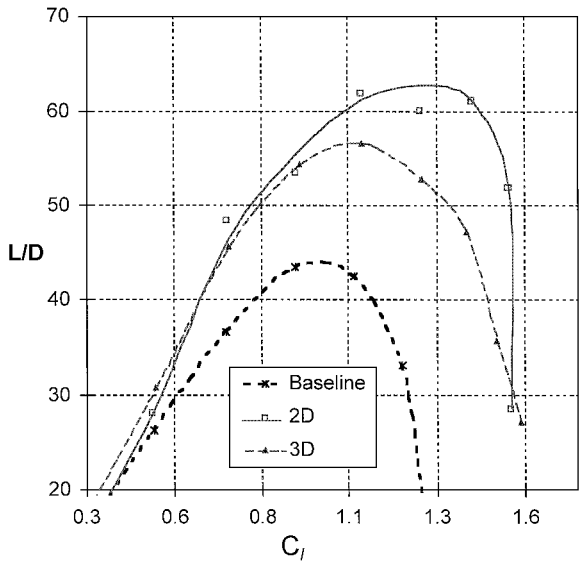

Fig. 4 Lift/drag ratio vs lift (tripped boundary layer, $R_c = 0.55 \times 10^6$, $F^+ = 1.2$).

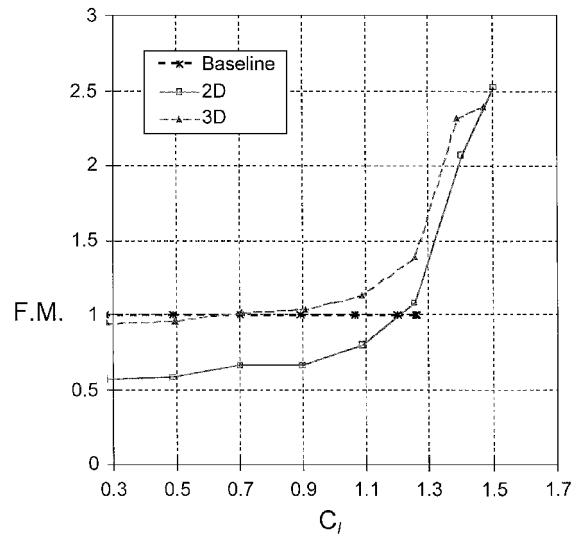

Fig. 5 FM vs lift (tripped boundary layer, $R_c = 0.55 \times 10^6$, $F^+ = 1.2$).

Observing the various aspects of the airfoil performance, one can identify the following trends.

1) $C_{l_{max}}$ increases by 20–22%, regardless of the excitation mode, because of the delay of stall by 2–4 deg. Considering the lower power consumption of the three-dimensional mode, it is certainly preferred for lift enhancement at landing configuration.

2) The two-dimensional mode generates a milder poststall behavior than the three-dimensional mode; therefore it is expected to perform better in hysteresis prevention and dynamic stall suppression.

3) The baseline drag diverges rapidly for $C_l > 0.7$; the drag divergence of the two-dimensional and three-dimensional excited modes is milder. At $C_l \geq 1.1$ the drag of the two-dimensional mode is the smallest.

4) The two-dimensional mode generates the highest L/D at the highest C_l. The combination of high C_l at the highest L/D and mild poststall behavior makes the two-dimensional mode a suitable candidate for takeoff configuration.

5) When power efficiency is considered, in conjunction with the FM (Fig. 5), it becomes evident that it is expedient to operate in the three-dimensional mode at $C_l > 0.7$ and in the two-dimensional mode at $C_l > 1.2$.

The physical mechanism describing the nature of spanwise and streamwise vorticity generation by the two-dimensional and three-dimensional modes and the interaction between the separating boundary layer and these disturbances was not studied. However, it is the first demonstration of energy-efficient active flow control.

Acknowledgments

The authors thank M. Shepshelovits, Israel Aircraft Industries, for permission to use and modify the airfoil, M. Goldberg for manufacturing the actuators and modifying the airfoil, and T. Bachar, T. Naveh, and E. Nevoh for assistance in developing the actuators and performing the experiments.

References

[1] Seifert, A., Darabi, A., and Wygnanski, I., "On the Delay of Airfoil Stall by Periodic Excitation," *Journal of Aircraft*, Vol. 33, No. 4, 1996, pp. 691–699.

[2] Seifert, A., and Pack, L. G., "Oscillatory Control of Separation at High Reynolds Numbers," AIAA Paper 0214-98, Jan. 1998; also *AIAA Journal* (submitted for publication).

[3] Rae, W. H., Jr., and Pope, A., *Low Speed Wind Tunnel Testing*, 2nd ed., Wiley, New York, 1984, pp. 349–361.

[4] Lin, J. C., Selby, G. V., and Howard, F. G., "Exploratory Study of Vortex-Generating Devices for Turbulent Flow Separation Control," AIAA Paper 91-0042, Jan. 1991.

M. Samimy
Associate Editor

Use of Analytical Flow Sensitivities in Static Aeroelasticity

Richard W. Newsome*
Allison Advanced Development Company, Indianapolis, Indiana 46206
and
Gal Berkooz† and Rajesh Bhaskaran‡
Beam Technologies, Inc., Ithaca, New York 14850

Introduction

MODERN computational fluid dynamics tools can be used to predict sensitivities for flows encountered by aircraft and missiles throughout the flight regime. In this study, we describe one important multidisciplinary application of aerodynamic sensitivity analysis, namely, the coupling of the aerodynamic sensitivities with a structural dynamics analysis and optimization code. Coupling aerodynamic and structural models provides a powerful tool for predicting and controlling both static and dynamic aeroelastic phenomena.

The flow is modeled using the two-dimensional Euler equations. The flow sensitivity is calculated using the sensitivity equation or the analytical sensitivity method. In this approach, equations for the sensitivities are formed by differentiating the flow-governing equations and boundary conditions and then discretizing. References 1 and 2 have previously applied the analytical sensitivity method to the Euler equations. Sensitivity solutions were carried out for two-dimensional subsonic and transonic flow over an airfoil. The sensitivity to change in geometry was incorporated into the ASTROS structural analysis code in place of linear aerodynamic (panel-method-based) sensitivity to calculate static aeroelastic effects in a noniterative fashion. Results are presented for a wing section in transonic flow mounted on a torsion spring for which the geometry variation is due to deformation as well as rotation.

Sensitivity Analysis

The sensitivity equations are obtained by differentiating the Euler equations with respect to the design variables d_k. Details of the

Received Nov. 7, 1996; revision received March 26, 1998; accepted for publication May 4, 1998.

* Systems Manager, F120 Engine Program, P.O. Box 7162, XB12. Associate Fellow AIAA.
† President, 110 N. Cayuga Street.
‡ Staff Scientist, 110 N. Cayuga Street. Member AIAA.

derivation of the sensitivity equations for the Euler equations are given in Ref. 2. The sensitivity equations are of the same form as the Euler equations but linear. Thus, one can amend an existing code for the Euler equations to solve the sensitivity equations by redefining the flux functions and boundary conditions.

The flow equations were solved using CFL2D, the two-dimensional version of the CFL3D code developed at NASA Langley Research Center.[3] This code uses a finite volume, upwind-biased formulation. The sensitivity equations (one set for each design variable) were solved using the same algorithm as in CFL2D with minor differences to obtain the sensitivity of the primitive flow variables $q' = (\rho', u', v', p')^T$, where $\rho' \equiv \partial\rho/\partial d_k$ etc. Roe's flux-difference splitting, used in CFL2D to calculate the interface fluxes, was reformulated for the sensitivity equation flux. In our case, the sensitivity equations remained the same for different design variables and changes came in only through the boundary and initial conditions. As in the flow solver algorithm, the sensitivity equations were time marched using a spatially split approximate factorization method. Because the eigenvalues and eigenvectors of the inviscid sensitivity flux Jacobians are identical to the flow flux Jacobians and the same for all sensitivity equation sets, they were precomputed and stored.

For the case where the design variables describe the deformation of the body surface, the development of the boundary conditions for the sensitivity equations is straightforward except on the deformable body surface where the boundary conditions are functionally dependent on the design variables.[2] Consider, for example, the specification of u'_w, where the subscript w denotes wall or surface value. For a two-dimensional flow, the boundary condition for u_w from flow tangency is of the form

$$u_w = a(x_\xi, y_\xi)u_1 + b(x_\xi, y_\xi)v_1 \tag{1}$$

where the subscript 1 denotes a value at the first cell centroid above the surface. Differentiating Eq. (1) with respect to d_k gives

$$u'_w = -\frac{\partial u_w}{\partial x}\frac{\partial x}{\partial d_k} - \frac{\partial u_w}{\partial y}\frac{\partial y}{\partial d_k} + \left(\frac{\partial a}{\partial d_k}u_1 + a\frac{\partial u_1}{\partial d_k}\right) + \left(\frac{\partial b}{\partial d_k}v_1 + b\frac{\partial v_1}{\partial d_k}\right) \tag{2}$$

The terms on the right-hand side are known from geometry and the known flow solution. Similar expressions hold for v'_w, p'_w, and ρ'_w.

Static Aeroelastic Analysis

The structural analysis results in a coupled set of ordinary differential equations (ODEs) describing the displacements $\{\delta\boldsymbol{x}\}$ at a discrete set of nodal points due to the forces $\{\boldsymbol{F}\}$ acting on the structure. The system of ODEs to be solved is

$$[M]\{\delta\ddot{\boldsymbol{x}}\}_s + [K]\{\delta\boldsymbol{x}\}_s = \{\boldsymbol{F}\}_s \tag{3}$$

where the subscript s denotes the structural coordinate system. In general, the aerodynamic and structural problems are coupled because $\{\boldsymbol{F}\}_s$ is a function of $\{\delta x\}_s$. Expanding $\{\boldsymbol{F}\}_s$ in a Taylor series and neglecting higher-order terms gives

$$[M]\{\delta\ddot{\boldsymbol{x}}\}_s + \left[[K] - \left[\frac{\partial \boldsymbol{F}}{\partial \boldsymbol{x}}\right]_s^o\right]\{\delta\boldsymbol{x}\}_s = \{\boldsymbol{F}\}_s^o \tag{4}$$

where $\{\boldsymbol{F}\}_s^o$ is the aerodynamic load on the undeformed structure. The preceding equation is similar to Eq. (3) except for a modified stiffness matrix and can be solved by modifying a standard structural finite element code.

Here the Harder–Desmarais spline interpolation method[4] is used because of its availability in ASTROS, the code used to perform the static aeroelasticity calculations. The interpolation relations are of the form

$$\{\delta\boldsymbol{x}\}_a = [G_{sa}]\{\delta\boldsymbol{x}\}_s, \qquad \{\boldsymbol{F}\}_s = [G_{as}]\{\boldsymbol{F}\}_a \tag{5}$$

where $[G_{sa}]$ and $[G_{as}]$ are the transformation matrices and the subscript a denotes the aerodynamic coordinate system. The aeroelastic increments on the two grids are related by

$$\{\delta\boldsymbol{F}\}_s = [G_{as}]\{\delta\boldsymbol{F}\}_a \tag{6}$$

where

$$\{\delta\boldsymbol{F}\}_a = \left[\frac{\partial \boldsymbol{F}}{\partial \boldsymbol{x}}\right]_a^o \{\delta\boldsymbol{x}\}_a \tag{7}$$

Several investigators have demonstrated the utility of Bezier–Bernstein polynomials for providing a compact representation of two-dimensional curves and three-dimensional surfaces.[5] Here the y-coordinate surface geometry is described by $N+1$ Bezier coefficients d_k:

$$y(\xi') = \sum_{k=0}^{N} d_k B_k^N(\xi') \quad \text{where} \quad B_k^N(\xi') = \frac{N!}{k!(N-k)!}\xi'(1-\xi') \tag{8}$$

and where ξ' is a parametric variable that runs along the surface and varies from 0 to 1. For an arbitrary surface geometry, the Bezier coefficients are obtained by minimizing the least-squares error between the Bezier fit and the coordinates at the cell face centroids. This leads to the formula (see Ref. 6)

$$\{d\} = [[N]^T[N]]^{-1}[N]^T\{y\} \tag{9}$$

where $\{d\}$ is the N-dimensional vector of the d_k corresponding to the M-dimensional vector $\{y\}$ of surface cell face centroids and $N_{ij} = B_j^N(\xi'_i)$.

The basic idea is to calculate the aeroelastic increment using the Bezier coefficients so that in place of Eq. (7) we use

$$\{\delta\boldsymbol{F}\}_a = \left[\frac{\partial \boldsymbol{F}}{\partial d}\right]_a^o \{\delta d\} \tag{10}$$

The matrix $[\partial\boldsymbol{F}/\partial d]_a^o$ is called the aerodynamic influence coefficient matrix. Combining Eqs. (5), (6), and (10) gives the following expression for the aeroelastic increment with only y displacements considered (see Ref. 7 for details):

$$\{\delta\boldsymbol{F}\} = [G_{as}]\left[\frac{\partial \boldsymbol{F}_a}{\partial d}\right]^o [[N]^T[N]]^{-1}[N]^T[G_{sa}]\{\delta y\} \tag{11}$$

Results

Sensitivity solutions were carried out for two-dimensional, inviscid, subsonic and transonic flow over an RAE 2822 airfoil. The sensitivity equation solver was implemented by modifying the CFL2D code. A C grid consisting of 129×49 points and extending 20 chord lengths outward from the body was used. Freestream boundary conditions were specified at the outer boundary of the C grid. Across the wake, continuity boundary conditions were applied. The streamwise variation of the flow and sensitivity variables was set to zero at the outflow boundary. A single 17th-order Bezier polynomial was chosen to represent the RAE 2822 airfoil. To simplify the problem, it was assumed that the structure deformed only in the y direction.

To validate the sensitivity solution for geometry variation, a small change in the angle of attack was modeled as a geometry change, and the change in pressure coefficient was calculated using

$$\Delta C_p \simeq \sum_{k=0}^{N+1} \frac{\partial C_p}{\partial d_k}\Delta d_k \tag{12}$$

This result was compared with that obtained by taking the difference in the pressure coefficients predicted by the flow solver at the two angles of attack. Figure 1 shows the comparison for a 0.05-deg pitch up and pitch down about the 30% chord location at Mach 0.75 and $\alpha = 2.72$ deg. It is seen that the agreement in both cases is quite good. Because the solution is discontinuous at the shock location, the sensitivity there is not defined.

The ASTROS structural code developed at the Air Force Research Laboratory and documented in Ref. 8 was used to solve Eq. (4) to account for static aeroelastic effects. A representative structural model consisting of surface, web, and spar elements was constructed for a wing section with a chord-to-span ratio arbitrarily set at 20:1 (because the sensitivity calculations were two dimensional). Static aeroelastic solutions were generated at Mach 0.50 and 0.75. For the

Table 1 Summary of normal force coefficients

Mach number	K_θ	$C_{y,\text{rigid}}$	$C_{y,\text{splined}}$	$C_{y,\text{flex}}$	$C_{y,\text{flex}}/C_{y,\text{rigid}}$
0.50	3.89	0.62888	0.64973	0.61133	0.9409
0.75	10.37	0.94747	0.96402	0.93634	0.9713
0.75	25.94	0.94747	0.96402	0.94842	0.9839

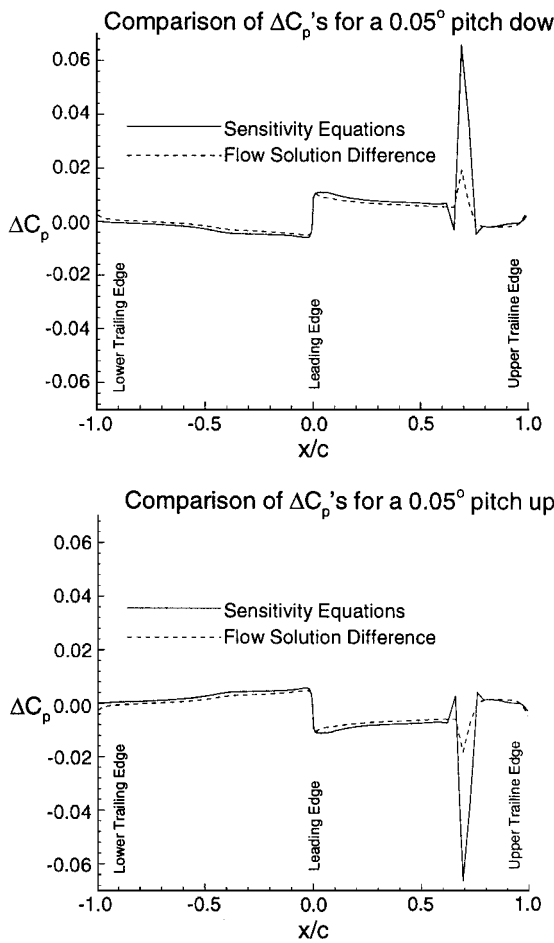

Fig. 1 Comparison of ΔC_p at Mach 0.75 and 2.72-deg angle of attack.

material properties selected, the two-dimensional model showed very little deformation and a small aeroelastic increment. To better demonstrate the integration of the sensitivity analysis with the structural analysis, the structural model was modified to include a torsional spring at a 30% chord fixed mount point. Because the center of pressure was at 38% and 41% of chord for the Mach 0.5 and 0.75 cases, respectively, the airload produced a nose-down pitching moment. This provided a realistic approximation to the torsional effects on the outboard sections of a three-dimensional wing. The resulting displacements were then primarily due to rotation rather than deformation. The spring constant K_θ was adjusted to provide deflections within which the linearization assumption was expected to provide reasonable answers.

The structural displacements on the upper surface, nondimensionalized by the chord length, without and with aeroelastic feedback at the transonic Mach number of 0.75 and $K_\theta = 25.94$ (nondimensionalized by the product of chord, planform area, and freestream dynamic pressure), are shown in Fig. 2. The displacements show the expected aeroelastic relief effect in which the equilibrium solution reflects the weakening of the aerodynamic moment in response to the decreased angle of attack. The normal force coefficients with and without aeroelastic feedback for the different cases considered are listed in Table 1. The quantities $C_{y,\text{rigid}}$ and $C_{y,\text{splined}}$ are the normal force coefficients for the undeformed wing in the aerodynamic and structural coordinate systems, respectively, and $C_{y,\text{flex}}$ is the normal force coefficient with aeroelastic feedback. Table 1 highlights that

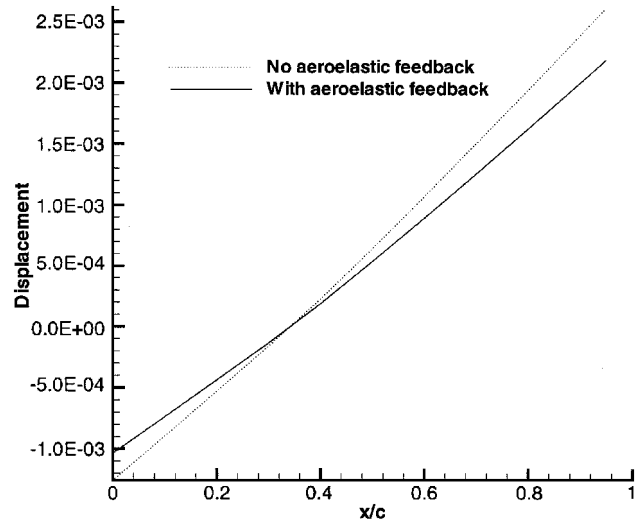

Fig. 2 Nondimensional structural displacements on the upper surface without and with aeroelastic feedback at Mach number of 0.75.

the inaccuracies in the Harder–Desmarais spline interpolation are of the same order as the aeroelastic force increment. This problem can be overcome by using more accurate interpolation methods.

Conclusion

A finite volume, upwind-biased sensitivity equation solver for the Euler equations was developed by modifying an existing flow solver. The solver was used to calculate the sensitivity of subsonic and transonic flows to changes in geometry. The calculated sensitivities were used to carry out a static aeroelastic analysis for a wing section in transonic flow undergoing rotation and deformation. A deficiency in the accurate interpolation of loads and displacements between the aerodynamic and structural domains was identified as an area for improvement. Both the sensitivity and the coupling methods can be extended to three dimensions. The range of applicability includes static, loosely coupled, aeroelastic interactions in which the linear sensitivity solutions accurately describe the aerodynamic response to structural deformation.

Acknowledgments

This work was supported by Contract F49620-95-C-0027 from the U.S. Air Force Office of Scientific Research monitored by S. Schreck and Contract WL F33615-95-C-3227 from the Structures Directorate at Wright Laboratories monitored by L. Hutsell. The integration of the sensitivities into ASTROS was performed by Mike Love and Dan Barker of Lockheed Martin, with whom we had many useful discussions, and their help is gratefully acknowledged.

References

[1] Beux, F., and Dervieux, A., "Exact-Gradient Shape Optimization of a 2-D Euler Flow," *Finite Elements in Analysis and Design*, Vol. 12, Nos. 3, 4, 1992, pp. 281–302.

[2] Borggaard, J., and Burns, J., "A PDE Sensitivity Equation Method for Optimal Aerodynamic Design," *Journal of Computational Physics*, Vol. 136, No. 2, 1997, pp. 366–384.

[3] Vatsa, V. N., Thomas, J. L., and Wedan, B. W., "Navier–Stokes Computations of Prolate Spheroids at Angle of Attack," AIAA Paper 87-2627, Aug. 1987.

[4] Harder, R. L., and Desmarais, R. N., "Interpolation Using Surface Splines," *Journal of Aircraft*, Vol. 9, No. 2, 1972, pp. 189–191.

[5] Burgreen, G. W., Baysal, O., and Eleshaky, M. E., "Improving the Efficiency of Aerodynamic Shape Optimization," *AIAA Journal*, Vol. 32, No. 1, 1994, pp. 69–76.

[6] Press, W. H., Teukolsky, S. A., Vetterling, W. T., and Flannery, B. P., *Numerical Recipes in FORTRAN*, 2nd ed., Cambridge Univ. Press, Cambridge, England, UK, 1992, pp. 665–675.

[7] Bhaskaran, R., and Berkooz, G., "Optimization of Fluid-Structure Interaction Using the Sensitivity Equation Approach," *Proceedings of the 4th International Symposium on Fluid-Structure Interactions, Aeroelasticity, Flow-Induced Vibration and Noise*, Vol. 1, American Society of Mechanical Engineers, New York, 1997, pp. 49–56.

[8]Johnson, E. H., and Venkayya, V. B., "Automated Structural Optimization System (ASTROS), Vol. 1, Theory Manual," U.S. Air Force Wright Aeronautical Lab., AFWAL TR-88-3028, Wright–Patterson AFB, OH, Dec. 1988.

J. Kallinderis
Associate Editor

Limit Cycle Measurements from a Cantilever Beam Attached to a Rotating Body

Christopher L. Lee*
Lawrence Livermore National Laboratory, Livermore, California 94551

I. Introduction

THE simple model of a cantilever beam attached to a rigid, rotating body has been studied extensively inasmuch as it captures the characteristic dynamics of flexible rotating mechanical systems such as helicopter blades, robot arms, and satellite appendages. Some studies have focused on nonlinear dynamic response. The results of one such study,[1] which examined the internally resonant response under periodic, near-resonant excitation, identified distinct classes of periodic responses. Saddle node, pitchfork, and Hopf bifurcation points, associated with the existence and exchange of stability of periodic solutions, were located in the system parameter space. Additionally, the Hopf bifurcation points also indicate regions where stable limit cycle responses characterized as an amplitude modulated time series may exist.[2]

This Note describes the measurement of a stable limit cycle response in an experimental study of the dynamics of a cantilever beam attached to a rotating body. The limit cycle is an amplitude modulated response that would appear near Hopf bifurcations predicted in the theoretical study. A periodic response is presented first. Then as a single-system parameter (the excitation frequency) is varied, the periodic response loses stability and gives way to a stable limit cycle. Such behavior is characteristic of limit cycle (amplitude modulated motion on a two torus) responses measured in other mechanical systems.

II. Experimental Study

A. Apparatus

A schematic diagram of the apparatus is shown in Fig. 1 and consists of the following: a) vacuum vessel, aluminum tank that is evacuated to eliminate aerodynamic loads; b) flexible beam, Lexan, length = 0.52 m, Young's modulus = 2375 MPa, density = 1200 kg/m^3; c) rigid body, solid, aluminum hub, radius $R = 0.076$ m; mounted to a steel drive shaft, the beam is bolted to the rigid body creating a fixed boundary condition; d) four accelerometers, Endevco 7250 A/AM-10 (mass = 1.8 g each), mounted at two locations along the length of the beam with each pair mounted normal to motion in the flapping (out of the plane of rotation) or lead/lag (in the plane of rotation) directions; e) vibration exciter, generic audio speaker mounted vertically to excite motion in the flapping direction only; f) load cell, Wilcoxon Research 5969, mounted on the beam and connected to the exciter by a short, stiff stinger; g) slip ring, 36 channels allowing wire-free connection for signals from the accelerometers, exciter, and load cell; h) electric motor, Parker Hannifin OEM650 Microstep Drive with OEM83-135-MO step motor run at 25,000 steps/revolution; i) motor controller, Galil DMC-1010 motion controller card in personal computer; j) data acquisition and analysis computer; and k) signal generator/analyzer, HP3566A.

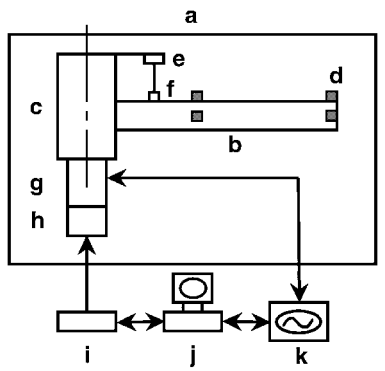

Fig. 1 Schematic of experimental apparatus.

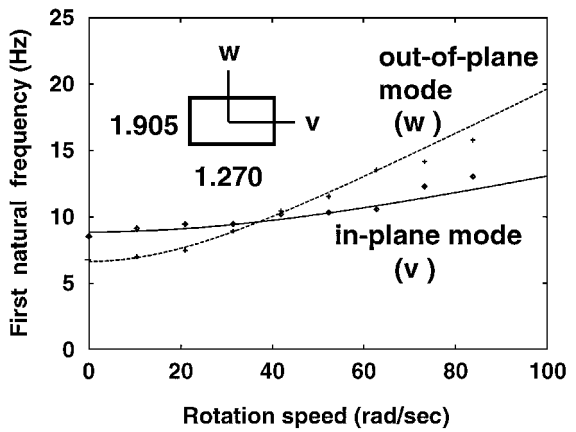

Fig. 2 First natural frequency (theoretical/experimental) of the first in-plane (——/♦) and out-of-plane (– – –/+) bending modes for a beam with a rectangular cross section. The natural frequencies are equal when the rotation speed is 36.9 rad/s.

B. Measurement Conditions

A beam with a rectangular cross section is used. At rest, the natural frequencies in the lead/lag and flapping directions of the beam are not equal. For the class of beams in which the moment of inertia is greater in the lead/lag direction than in the flapping direction, the natural frequencies of lead/lag modes are greater than those of corresponding flapping modes. As the beam rotates, the centrifugal force stiffens the beam in the lead/lag and flapping directions at different rates. As a result for this class of beams, there exists a speed at which the natural frequencies of a lead/lag and a flapping mode are equal.

As shown in Fig. 2, for a beam with a cross section of 1.270 × 1.905 cm the first natural frequencies are commensurable in a 1:1 ratio at an angular speed of 36.9 rad/s (353 rpm). In Fig 2, the solid and dashed lines represent theoretical predictions, whereas the diamonds and crosses represent measurements taken from an experimental modal analysis survey.[3] Two pairs of accelerometers are attached to the beam at the tip and at an arbitrary midpoint. Time histories from the accelerometers are recorded using the signal analyzer. The analyzer also provides a specified harmonic excitation to the vibration exciter.

C. Sample Results

Two examples are presented here to illustrate the measurement of a typical periodic response and its transition into a limit cycle response. In these examples, the hub rotation speed is a constant 39.94 rad/s (≈350 rpm). In the first example, the excitation frequency is 9.6875 Hz. Figure 3a shows a portion of the time history recorded from the accelerometer near the free end of the beam in the flapping direction. The time history in the lead/lag direction (not shown) has a similar appearance.

Figure 3b shows a fast Fourier transform (FFT) spectrum of the time history. The frequency peak with the greatest amplitude occurs at 9.6875 Hz, which is the excitation frequency. The peak immediately to the right occurs at 9.87 Hz and corresponds to the natural frequency of the flapping mode. The other peaks correspond to the vacuum tank and its harmonics. From the modal survey, the natural

Received Jan. 8, 1998; revision received April 18, 1998; accepted for publication April 22, 1998.

*Engineer, Structural Mechanics Group, New Technologies Engineering Division, Box 808, L-126.